

Catalytic Reduction of a Tetrahydrobiopterin Radical within Nitric-oxide Synthase*

Received for publication, November 12, 2007, and in revised form, February 15, 2008. Published, JBC Papers in Press, February 18, 2008, DOI 10.1074/jbc.M709250200

Chin-Chuan Wei^{†1}, Zhi-Qiang Wang^{§¶}, Jesús Tejero[§], Ya-Ping Yang[§], Craig Hemann^{||}, Russ Hille^{**}, and Dennis J. Stuehr^{§2}

From the [§]Department of Pathobiology, The Lerner Research Institute, Cleveland Clinic Foundation, Cleveland, Ohio 44195, the [†]Department of Chemistry, Southern Illinois University Edwardsville, Edwardsville, Illinois 62026, the [¶]Department of Chemistry, Kent State University-Tuscarawas, New Philadelphia, Ohio 44663, the ^{**}Department of Biochemistry, University of California, Riverside, California 92521, and the ^{||}Department of Molecular and Cellular Biochemistry, Ohio State University, Columbus, Ohio 43210

Nitric-oxide synthases (NOS) are catalytically self-sufficient flavo-heme enzymes that generate NO from arginine (Arg) and display a novel utilization of their tetrahydrobiopterin (H₄B) cofactor. During Arg hydroxylation, H₄B acts as a one-electron donor and is then presumed to redox cycle (*i.e.* be reduced back to H₄B) within NOS before further catalysis can proceed. Whereas H₄B radical formation is well characterized, the subsequent presumed radical reduction has not been demonstrated, and its potential mechanisms are unknown. We investigated radical reduction during a single turnover Arg hydroxylation reaction catalyzed by neuronal NOS to document the process, determine its kinetics, and test for involvement of the NOS flavoprotein domain. We utilized a freeze-quench instrument, the biopterin analog 5-methyl-H₄B, and a method that could separately quantify the flavin and pterin radicals that formed in NOS during the reaction. Our results establish that the NOS flavoprotein domain catalyzes reduction of the biopterin radical following Arg hydroxylation. The reduction is calmodulin-dependent and occurs at a rate that is similar to heme reduction and fast enough to explain H₄B redox cycling in NOS. These results, in light of existing NOS crystal structures, suggest a “through-heme” mechanism may operate for H₄B radical reduction in NOS.

Nitric-oxide synthases (NOS,³ EC 1.14.13.39) are flavo-heme enzymes that catalyze a stepwise oxidation of L-arginine (Arg)

to form nitric oxide (NO) and L-citrulline (1, 2) (Fig. 1). Arg is first hydroxylated by NOS in an NADPH- and O₂-dependent reaction to form N^ω-hydroxyl-L-arginine (NOHA) as an enzyme-bound intermediate. NOHA is then oxidized by NOS to citrulline and NO in a second NADPH- and O₂-dependent reaction. The reactions take place within the NOS oxygenase domain dimer (NOSoxy), which contains bound protoporphyrin IX (heme) and 6-(R)-tetrahydrobiopterin (H₄B).

The NOS heme catalyzes oxygen activation by a mechanism that is similar to that described for cytochrome P450 (3). However, in NOS the electron required for ferric heme reduction is provided by an attached flavoprotein domain that contains FAD, FMN, and an NADPH binding site, and heme reduction is dependent on calmodulin (CaM) binding (1, 2). NOS enzymes also require H₄B as a cofactor. H₄B is bound tightly within NOS enzymes (*k*_{off} ranges from 0.07 to 1.6 min⁻¹ at 37 °C) (4, 5), and this enables H₄B to remain bound in NOS through multiple catalytic turnovers (6–8). Moreover, H₄B performs a novel redox function in NOS: it reduces the ferric heme-superoxy intermediate (Fe^{III}O₂⁻) that forms during oxygen activation, and becomes an enzyme-bound H₄B radical in the process (9–13). Electron transfer from H₄B is critical because it enables NOS to form the heme-oxy species that react with Arg or NOHA (1, 2) (Fig. 1).

Several studies suggest that the H₄B radical remains in NOS after it forms and must be reduced back to H₄B in order for the enzyme to continue catalysis (1, 2) (Fig. 1). However, the fact that bound H₄B radical undergoes a time-dependent oxidation (10, 12, 13), and that NOHA can dissociate from NOS after it forms (14, 15), places a time constraint on H₄B radical reduction. Following Arg hydroxylation, the H₄B radical remains in the ferric enzyme (Fig. 1, *enzyme species III*), and thus its reduction should require an electron from the NOS flavoprotein domain (1, 2) (Fig. 1, *enzyme species III* and *IV*). The validity of this process and its regulation are unclear.

Because CaM binding to NOS enables the flavoprotein domain to transfer electrons to the oxygenase domain heme (16), we hypothesized that reduction of the H₄B radical following Arg hydroxylation may also require CaM binding to NOS.

* This work was supported in part by National Institutes of Health Grants CA53914, GM51491, and HL58883 (to D. J. S.) and ES012658 and GM075036 (to R. H.), American Heart Association Beginning Grant-in-aid 0365175B and a Cottrell Science College Award from Research Corporation (to C.-C. W.), American Heart Association Beginning Grant-in-aid 0565297B (to Z.-Q. W.), and American Heart Association Postdoctoral Fellowship 0625632B (to J. T.). The costs of publication of this article were defrayed in part by the payment of page charges. This article must therefore be hereby marked “advertisement” in accordance with 18 U.S.C. Section 1734 solely to indicate this fact.

¹ To whom correspondence may be addressed: Dept. of Chemistry, Southern Illinois University Edwardsville, Edwardsville, IL 62026. Tel.: 618-650-2454; Fax: 618-650-3556; E-mail: cwei@siue.edu.

² To whom correspondence may be addressed: Dept. of Pathobiology, NC-22, Lerner Research Institute, The Cleveland Clinic Foundation, 9500 Euclid Ave., Cleveland, OH 44195. Tel.: 216-445-6950; Fax: 216-636-0104; E-mail: stuehrd@ccf.org.

³ The abbreviations used are: NOS, nitric-oxide synthase; NOSoxy, NOS oxygenase domain; NOSred, NOS reductase domain; NOHA, N^ω-hydroxyl-L-arginine; H₄B, (6R)-5,6,7,8-tetrahydro-L-biopterin; 5MeH₄B, (6R)-5-methyl-

6,7,8-trihydro-L-biopterin; Fe^{III}O₂⁻, heme ferric superoxy intermediate; EPPS, N-(2-hydroxyethyl)-piperazine-N'-3-propanesulfonic acid; FSQ, flavin semiquinone; EPR, electron paramagnetic resonance; CaM, calmodulin; nNOS, neuronal NOS.

To explore this possibility, we developed a means to monitor the extent and kinetics of pterin radical reduction in NOS after Arg hydroxylation occurs. Our experiments manipulate free Ca^{2+} levels so as to allow or prevent the CaM-dependent electron transfer between the NOS flavoprotein and oxygenase domains, as we have done previously (17). We also utilize an EPR technique that can distinguish the radical signals arising from the bound pterin *versus* the NOS flavins during the reaction. Our results provide the first example of enzyme-catalyzed pterin radical reduction in biology, and lay a foundation to explore its mechanism and regulation in the NOS enzymes.

EXPERIMENTAL PROCEDURES

Chemicals— H_4B , H_2B , and 5-methyl- H_4B (5Me H_4B) were obtained from Dr. Schirck's laboratory (Jona, Switzerland). A 5Me H_4B stock solution was prepared fresh in 40 mM EPPS, pH 7.5. All other chemicals were obtained either from Sigma or Fisher Scientific International, Inc.

UV-visible Spectrometry—Conventional spectra were obtained using a Cary 100 BIO instrument (Varian, Inc) equipped with temperature control and automatic stirring.

Protein Purification—Rat nNOS was overexpressed in *Escherichia coli* and was purified in the absence of H_4B as described previously (18, 19). The enzyme concentration was determined from the 444-nm absorbance of the ferrous-CO complex using an extinction coefficient of $76 \text{ mM}^{-1} \text{ cm}^{-1}$. The individual nNOSoxy and flavoprotein domains were overexpressed and purified as described previously (19, 20). The concentrated proteins were stored in a buffer containing 50 mM EPPS, pH 7.5, 2 mM β -mercaptoethanol, 10% glycerol, and 0.25 M NaCl.

Protein Sample Preparation—Ferrous nNOS was prepared by reducing CaM-bound ferric enzyme with NADPH in a gas-tight cuvette under anaerobic conditions as described previously (19, 20). Briefly, a buffered solution containing $\sim 120 \mu\text{M}$ nNOS, 10 mM Arg, 2 mM 5Me H_4B (or 1 mM H_2B), 200 μM CaM, and 600 μM Ca^{2+} was made anaerobic by several cycles of vacuum and flushing with deoxygenated N_2 , and then had N_2 -purged NADPH solution added to give 0.1 to 0.2 mM NADPH. Heme reduction was monitored by the appearance of a 550-nm absorbance peak and the disappearance of the 650-nm absorbance peak. After heme reduction was judged to be complete, we added additional NADPH to give a concentration of $\sim 1 \text{ mM}$. In some cases, an anaerobic EDTA solution was then added to the ferrous NOS sample to give 1.2 mM EDTA to release the bound CaM from the ferrous nNOS. The samples were periodically scanned in the UV-visible spectrophotometer to assure that the ferrous heme did not oxidize to ferric heme prior to transfer to the rapid quench instrument.

Rapid-freeze Kinetic Experiments—Ferrous nNOS samples prepared as described above were transferred with an anaerobic syringe to a rapid quench instrument (RQF-63, TKG Scientific, Bradford on Avon, UK) maintained at 10 °C, and the samples were rapid-mixed with an O_2 -saturated buffer (40 mM EPPS, 125 mM NaCl, pH 7.5) to initiate the reaction (this resulted in a post-mix O_2 concentration in the reaction of $\sim 0.8 \text{ mM}$). The reaction mixture was then aged for various times in the instrument followed by rapid injection into a liquid N_2 /isopentane freezing solution as described elsewhere (21). Some replicate

reactions utilized H_2B -bound nNOS in the rapid-freeze EPR study, to exclusively monitor the flavin semiquinone (FSQ) radical during the single turnover reaction. (H_2B does not form a radical in NOS during catalysis; Refs. 13, 21.) Three different nNOS preparations were used in the experiments, and each nNOS preparation was reacted under the CaM-bound and CaM-free condition on the same day.

EPR Analysis—Electron paramagnetic resonance (EPR) spectra of each frozen reaction sample was recorded in a Bruker ER300 instrument equipped with an ER 035 NMR gauss meter and a Hewlett-Packard 5352B microwave power controller. Temperature control was achieved using Oxford Instruments ESR 900 continuous-flow liquid helium cryostat and ITC4 temperature controller. All spectra were recorded at 150 K using a microwave power of 2 milliwatts or 20 microwatts, a frequency of 9.5 GHz, a modulation amplitude of 5 G, and a modulation frequency of 100 kHz.

The EPR spectrum of the 5Me H_4B radical was obtained by mixing 5Me H_4B -bound ferrous nNOSoxy with O_2 -saturated buffer and then rapid freezing after 125 ms of reaction as performed previously (12). The EPR spectral properties of the flavin semiquinone radical (FSQ) were recorded for the nNOS flavoprotein domain (20) and for the H_2B -bound, nNOS full-length protein (24). The FSQ radical was generated in either protein by adding a slight molar excess of NADPH to each protein in air-saturated buffer and then waiting for the flavins to air oxidize, while monitoring FSQ formation in a UV-visible spectrophotometer as a broad peak centered near 600 nm (20). This procedure results in both proteins containing an air-stable FMN semiquinone radical (20, 24).

The microwave power dependence of each radical signal was analyzed using nonlinear regression in Equation 1,

$$\text{Log}(S/\sqrt{P}) = -b/2\text{log}(P_{1/2} + P) + b/2\text{log}(P_{1/2}) + \text{log}(A) \quad (\text{Eq. 1})$$

where P is the power, S is the EPR intensity from double integration, $P_{1/2}$ is the power at half-saturation, A is a scaling factor, and b is an inhomogeneity parameter. All fittings were performed using Origin Pro 7.5 (OriginLab, Northampton, MA).

Determining the Concentrations of 5Me H_4B and FSQ Radicals—The primary EPR spin concentration was determined using Cu(II)EDTA solutions of known concentration, and their EPR spectra recorded under conditions as described here and in earlier reports (21, 27). The concentration of the FSQ radical was determined based on a comparison with EPR signals from samples of the 1-electron-reduced nNOS flavoprotein domain, whose total concentration and FSQ concentration were determined by UV-visible spectroscopy using known extinction coefficients (35). The dilution factors we used for correcting EPR signal intensities in the rapid-freeze-quench samples at each delay time were determined as done previously (21, 25). Briefly, a 500 μM Cu(II)EDTA solution was rapid-mixed with buffer at each delay time, subject to rapid freezing, and then the EPR signal intensities of these samples were measured. The dilution factors ranged from 2–3-fold.

The EPR intensities contributed by the 5Me H_4B and FSQ radical in each reaction sample were calculated using Equations

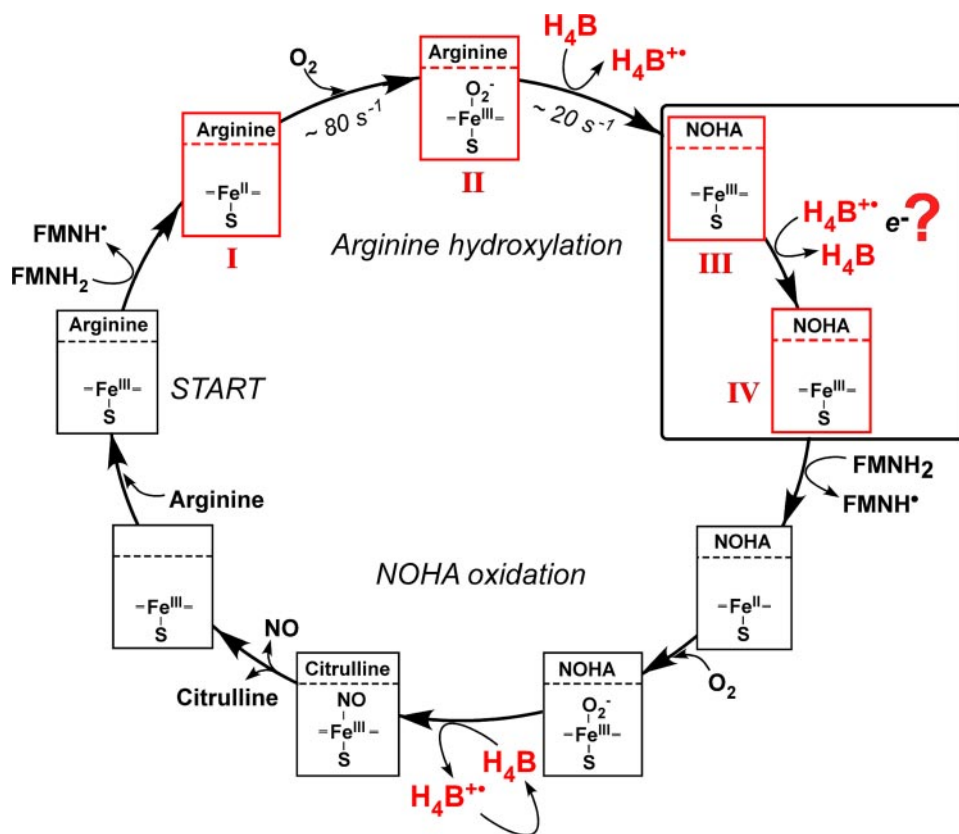


FIGURE 1. **Reaction scheme for NOS enzymes.** Some steps involved in Arg hydroxylation and NOHA oxidation are shown. The boxes indicate the heme species and the substrate or product that is bound at each step. Electrons are provided to the heme at discrete points by the flavoprotein domain (FMNH₂) or by H₄B, with their redox transformations as indicated. Red boxes are the steps in the reaction that occur in our single turnover reactions. The large box with question mark highlights the H₄B radical reduction step that is thought to follow Arg hydroxylation and is the focus of our study. See text for details.

2 and 3 and assuming that (i) one heme, one 5MeH₄B, one FAD, and one FMN molecule were bound in each subunit of the nNOS homodimer, and (ii) only two radical species were formed (see "Results").

$$I_{(2 \text{ milliwatts}, t)} = I_{H_4B, t} + I_{FSQ, t} \quad (\text{Eq. 2})$$

$$I_{(20 \text{ microwatts}, t)} = 0.1075 \times I_{H_4B, t} + 0.4843 \times I_{FSQ, t} \quad (\text{Eq. 3})$$

where $I_{(2 \text{ milliwatts}, t)}$ and $I_{(20 \text{ microwatts}, t)}$ were the double integrations of EPR spectra of the same sample measured at 2 milliwatts and 20 microwatts power at time t , respectively. $I_{H_4B, t}$ and $I_{FSQ, t}$ are only the two variables representing the intensities of 5MeH₄B and FSQ radicals at 2 milliwatts. The coefficients of 0.1075 and 0.4842 in Equation 3 were determined from power saturation measurements, indicating the fold intensity dropped from 2 milliwatts to 20 microwatts. By solving Equations 2 and 3, the EPR intensities from H₄B and FSQ at time t could be determined. The 5MeH₄B and FSQ radicals saturate at different microwave power: At 2 milliwatts the FSQ radical is largely saturated and no longer responsive to power, whereas the 5MeH₄B radical is not saturated at 2 milliwatts. The intensities we derived from Equations 2 and 3 were then converted to the concentration of individual radicals by comparison with samples of known radical concentration prepared as described above and measured at the same power setting. For example,

$I_{H_4B, t}$ is used to determine the concentration of the 5MeH₄B radical by comparison with data from Cu(II)EDTA samples of known concentrations, and $I_{FSQ, t}$ is used to determine the concentration of the FSQ radical by comparison of data from an authentic sample of nNOS flavoprotein FSQ radical in which its radical concentration was determined by UV-visible spectrometry. Therefore, variables in Equations 1 and 2 already embed the different power saturation behaviors of the 5MeH₄B and FSQ radicals.

Redox State of Bound Biopterin—The oxidation state of biopterin in CaM-bound or CaM-free nNOS samples following single catalytic turnover Arg hydroxylation reactions was determined using established methods (13, 22) with some modifications. Approximately 70 μM nNOS protein was incubated with 0.4 mM H₄B and 10 mM Arg at room temperature for 20 min and then passed through a PD-10 desalting column. Arg was then added to the protein to give a final concentration of 10 mM. A portion of the sample also received 100 μM CaM and 1 mM CaCl₂, while another portion received 3 mM EDTA. The samples

were made anaerobic and then reduced to ferrous by titrating with a near stoichiometric amount of dithionite solution. Approximately 0.3 ml of each anaerobic protein sample was mixed at room temperature with an equal amount of O₂-saturated buffer (40 mM EPPS, pH 7.5) containing 24 μl of iodine solution (0.9% (w/v) iodine in H₂O), and then was treated with standard alkaline and acidic iodine solutions used to determine concentrations of oxidized and reduced biopterin (22). After removing the precipitated protein by centrifugation, a 50-μl aliquot from each sample was then injected onto a 4.5 × 250-mm Partisil 5μ ODS-3 column (Alltech) that was equilibrated with an aqueous 5% MeOH solution. The content of H₄B and its oxidation products were determined by HPLC with fluorescence detection. The percentage of H₄B in the samples was calculated by subtracting the area of the peak eluting at 12 min in the aliquot that had undergone basic workup from the corresponding peak area present in the companion aliquot that had undergone acidic workup.

RESULTS

An H₄B radical forms in NOS during Arg hydroxylation to NOHA (Fig. 1, enzyme species I-III). A subsequent reduction of the H₄B radical is then thought to be required (Fig. 1, enzyme species III and IV) so that NOS can oxidize the bound NOHA to NO (Fig. 1). The reversible nature of CaM binding to nNOS (16,

17) enabled us to create two populations of ferrous nNOS (*i.e.* CaM-bound and CaM-free versions of species I in Fig. 1) for use in Arg hydroxylation reactions. Because only the CaM-bound nNOS can engage in electron transfer between its flavoprotein and oxygenase domain heme (16), this setup allowed us to test whether: 1) the H_4B radical that forms during Arg hydroxylation is actually reduced back to H_4B , 2) the nNOS flavoprotein domain provides the electron for H_4B radical reduction, and 3) the electron transfer to the H_4B radical requires that CaM is bound to nNOS.

We utilized nNOS because its flavoprotein-to-oxygenase domain electron transfer rate (about 4 s^{-1} at 10°C ; Ref. 19) and its H_4B radical formation rate during Arg hydroxylation (20 s^{-1} at 10°C) are the fastest among the three NOS enzymes, while the oxidative decay of its bound H_4B radical is the slowest (0.6 s^{-1} at 10°C) (12, 19). We also utilized $5MeH_4B$ in place of H_4B because it has an even faster radical formation (51 s^{-1}) and a slower oxidative decay (0.2 s^{-1}) in nNOS Arg hydroxylation reactions compared with H_4B (12), and thus provides the widest possible time window to observe reduction of the pterin radical in a NOS following Arg hydroxylation. The $5MeH_4B$ radical also has characteristic hyperfine structure that helps to distinguish it from flavin or superoxide radical species that may also form concurrently in NOS (9, 23–25).

In general, the reactions were initiated at 10°C by rapidly mixing an O_2 saturated buffer ($\sim 1.7\text{ mM } O_2$) with an anaerobic solution of NADPH pre-reduced CaM-bound or CaM-free ferrous nNOS ($\sim 0.12\text{ mM}$) that contained saturating concentrations of Arg and $5MeH_4B$. Following mixing, the reaction samples were aged for different times within the instrument and then underwent rapid freezing. The frozen reaction samples then had their free radical spectra and content analyzed by EPR. This procedure allowed us to study the sequential reaction steps I through IV (Fig. 1) during the Arg hydroxylation reaction catalyzed by nNOS. Under our reaction conditions, O_2 binding to the ferrous heme is rapid compared with subsequent H_4B radical formation and Arg hydroxylation, as indicated by the rates measured for these steps under near-identical reaction conditions (Fig. 1 and Refs. 12, 21, 25).

In our reactions we expect that EPR signals from the bound $5MeH_4B$ radical and from the FSQ radical will be present simultaneously during the course of the Arg hydroxylation reaction. Fig. 2 shows that this was the case. The figure contains representative EPR traces of reaction samples that were aged for the indicated times during an Arg reaction catalyzed by either CaM-free (*panel A*) or CaM-bound (*panel B*) nNOS. Standard EPR spectra of the $5MeH_4B$ radical and the nNOS FSQ radical are included in Fig. 2 for comparison. At 80 and 125 ms, the EPR traces have peak-to-trough values that range from 32 to 39 G. Because this value is close to the peak-to-trough value for authentic $5MeH_4B$ radical (40 G) and the traces otherwise display characteristic spectral features and hyperfine structure of the $5MeH_4B$ radical (9, 25), it appears to be the dominant radical present in the enzyme reaction samples at these two early time points. For the 1- and 2-s reaction samples, however, the peak-to-trough width declines to approach the value of the nNOS FSQ radical (20 G), and the spectral traces lose characteristic features that indicate a disappearance of the $5MeH_4B$

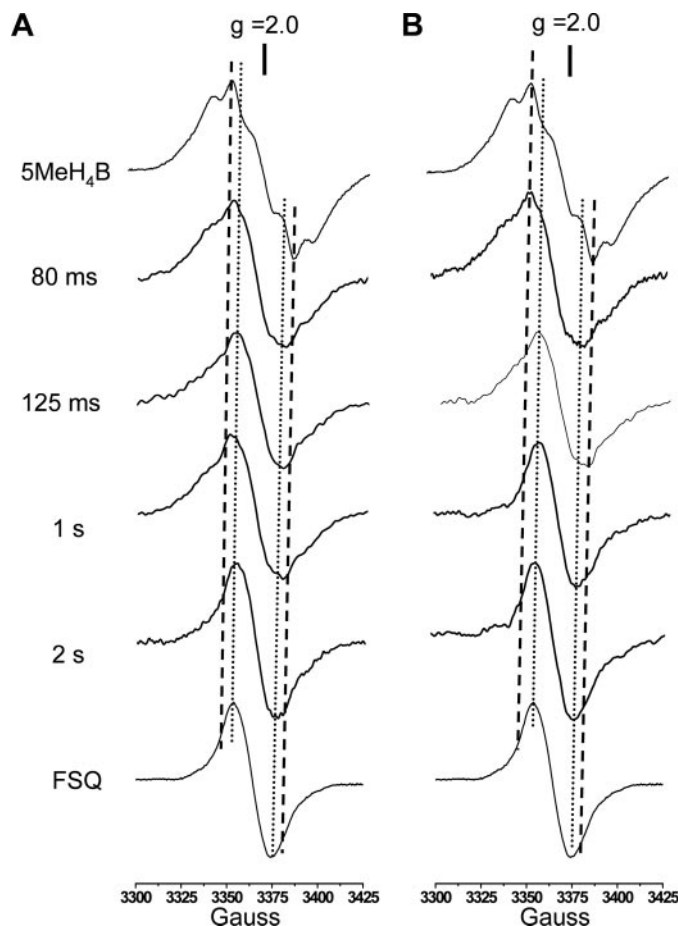


FIGURE 2. Representative EPR spectra of radicals detected during NOS reactions. Anaerobic solutions of ferrous nNOS containing $5MeH_4B$ and Arg were mixed with O_2 -saturated buffer to initiate the reaction in the absence (*panel A*) and presence (*panel B*) of bound CaM. Spectra of the nNOS $5MeH_4B$ radical and nNOS FSQ radical are included in each column for comparison. The *dashed* and *dotted* lines indicate the peak positions of authentic $5MeH_4B$ and FSQ radical signals, respectively. Data shown are representative of three independent experiments. The individual spectra are not meant to convey information regarding actual radical concentrations.

radical, particularly in the reaction catalyzed by the CaM-bound nNOS (*panel B*). The radical signals in these traces indicate the FSQ radical appears to become predominant in both reactions by 2 s (24, 26). Thus, a qualitative analysis of the traces suggest that the $5MeH_4B$ radical builds up and then begins to disappear within the 0 to 2 s reaction timeframe, concurrent with a more gradual and sustained buildup of the FSQ radical. Disappearance of the $5MeH_4B$ radical also appeared to be somewhat faster in the reaction catalyzed by CaM-bound nNOS compared with CaM-free nNOS (Fig. 2).

Because the reaction samples contained both FSQ and $5MeH_4B$ radical signals, we needed a way to assess their individual contributions. Conceivably, the power saturation profile of either radical could provide a means. We therefore determined the power saturation profiles for the $5MeH_4B$ and FSQ radicals when they were formed individually in nNOS. The $5MeH_4B$ radical was generated within nNOSoxy (12), which does not contain an attached flavoprotein domain, while the FSQ radical was generated within H_2B -bound, CaM-free nNOS. As shown in Fig. 3, the power saturation curves for the two radicals are clearly distinct. The $P_{1/2}$ value for the $5MeH_4B$

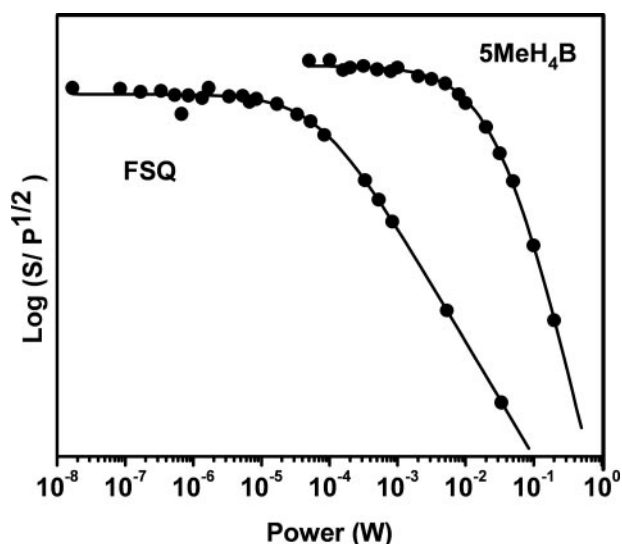


FIGURE 3. Power saturation curves of the 5MeH₄B and FSQ radicals of nNOS. The 5MeH₄B radical was generated in nNOSox while the FSQ radical was generated in H₂B-containing nNOS as described in the experimental section. Data were fit to Equation 1 to determine values of P_{1/2}. The values of P_{1/2}, A, and b were 38 milliwatts, 58.28, and 0.63 for 5MeH₄B, respectively and the values of P_{1/2}, A, and b were 65 microwatts, 340.23 and 0.55 for FSQ radical, respectively. Data are representative of two similar trials.

radical in nNOSox was 38 milliwatts, which is close to reported values for the H₄B radical in iNOSox and nNOS (10, 11, 27). The P_{1/2} value of the FSQ radical in nNOS was 65 microwatts, consistent with similar studies (24, 26).

Based on the power saturation profiles of the 5MeH₄B and FSQ radicals, there is a range of power values that can equally detect the intensity of either radical, and a different range of power values that favor detection of one radical over the other. For example, when the power changes from 2 milliwatts to 20 microwatts, the intensity of the 5MeH₄B and FSQ radical signals drop 9.3- and 2.1-fold, respectively. We therefore determined the total radical concentration (FSQ + 5MeH₄B) in each sample by integration of EPR spectra measured at 2 milliwatts, and calculated the FSQ contribution by integration of EPR spectra measured at a power of 20 microwatts. Using the equations described in the experimental section, we could then determine the separate concentration of the 5MeH₄B radical and FSQ radical in each reaction sample.

Fig. 4 shows the EPR signals that were present in a 125-ms reaction sample for CaM-free nNOS, and compares them with the EPR signals of authentic 5MeH₄B and FSQ radicals that were formed individually in nNOSox or nNOS, respectively. From the reaction sample spectra collected at 2 milliwatts and 20 microwatts power, we calculated the concentrations of the bound 5MeH₄B radical and flavin radical to be 119 ± 8 and 35 ± 8 μM, respectively, indicating that 85 ± 6% of the 5MeH₄B and 25 ± 6% of the flavins bound in nNOS were present in radical form at this time point.

To judge whether the analysis is reliable, we constructed the EPR signals present in a subset of the reaction samples by combining the signals recorded for authentic 5MeH₄B and FSQ radicals according to their relative contributions that we calculated for each time point, and then compared these constructed EPR traces to the actual signals that were observed for the same

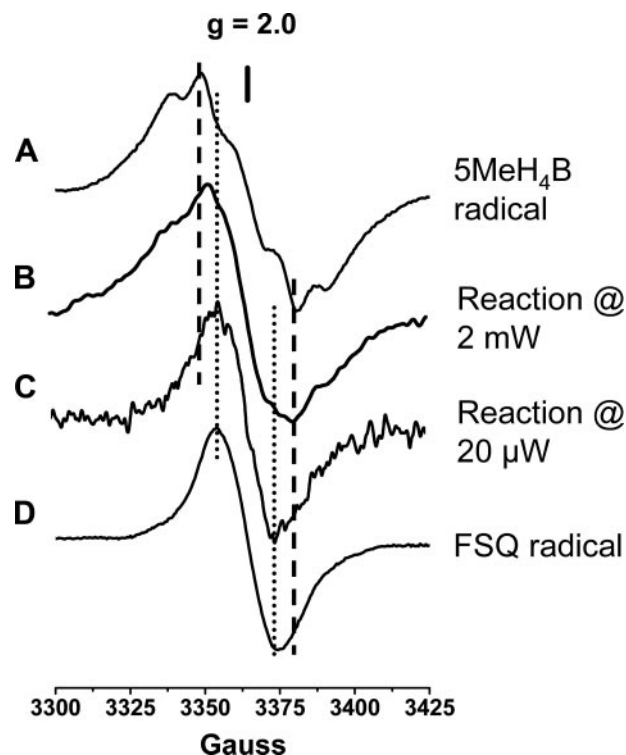


FIGURE 4. EPR spectra recorded at two microwave power settings for an Arg hydroxylation reaction. The reaction was that of CaM-free ferrous nNOS after 125 ms. Traces B and C, EPR spectra of the reaction sample recorded at 2 milliwatts and 20 microwatts, respectively. Traces A and D, EPR spectra of the authentic 5MeH₄B and FSQ radicals in nNOS. The dashed and dotted lines indicate a peak-to-trough signal width with 40 and 20 G, respectively. Data are representative of three independent experiments.

reaction samples. Fig. 5 compares the recorded and constructed EPR traces during a reaction of CaM-free nNOS. The constructed EPR spectra are in good agreement with the experimental traces, indicating that our analysis is reasonable and can determine the amounts of 5MeH₄B and FSQ radicals present in nNOS during the course of a single turnover reaction.

Regarding possible contributions from other radical species during the nNOS reaction, it has been demonstrated that EPR-detectable amounts of superoxide are released from the NOS heme when the single turnover reaction is uncoupled due to an absence of H₄B or Arg (10, 23). However, Arg and 5MeH₄B were present in our reactions at saturating concentrations and the nNOS single turnover reaction has been shown to be well coupled under this circumstance (12). Furthermore, the EPR spectrum of superoxide has a very high P_{1/2} value (~50 milliwatts) and a different line shape compared with the 5MeH₄B and FSQ radicals (23), and so should be easy to detect by our analysis. These considerations indicate a minimal superoxide release or buildup during our single turnover reactions.

We next utilized our EPR analysis to track 5MeH₄B and FSQ radical buildup and decay during single turnover Arg hydroxylation reactions catalyzed by CaM-bound versus CaM-free nNOS (Fig. 6). The data for 5MeH₄B radical formation and disappearance in both reactions are compared in Fig. 6A. The data were fit to the sequential kinetic reaction model, A to B to C (21) to obtain rates of 5MeH₄B formation and disappearance. The formation rates of the 5MeH₄B radical were similar in the

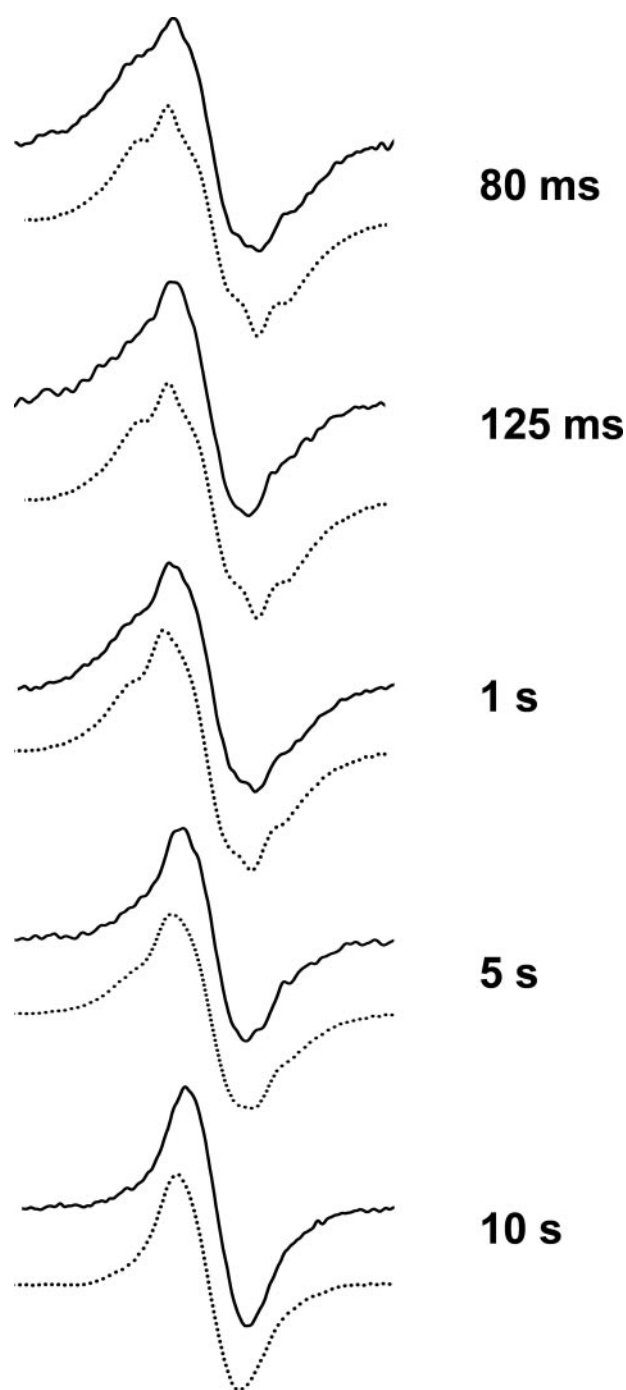


FIGURE 5. **Constructed versus actual EPR spectra obtained during Arg hydroxylation.** Actual traces that were recorded at the indicated times for a representative CaM-free nNOS reaction (solid lines) are compared with constructed EPR spectra (dashed lines) that represent weighted sums of the individual spectra for flavin and pterin radicals determined from individual signal contributions of the 5MeH₄B and FSQ radicals as explained under "Experimental Procedures."

CaM-free and CaM-bound nNOS reactions (80 ± 20 and $68 \pm 25 \text{ s}^{-1}$, respectively). In contrast, the disappearance rate of the 5MeH₄B radical was about 5 times faster in the CaM-bound nNOS reaction ($1.3 \pm 0.2 \text{ s}^{-1}$) than in the CaM-free nNOS reaction ($0.25 \pm 0.04 \text{ s}^{-1}$). The rate of radical disappearance in the CaM-free nNOS reaction is similar to the rate of 5MeH₄B radical oxidation in nNOSox (0.2 s⁻¹) following a single turnover Arg hydroxylation (12).

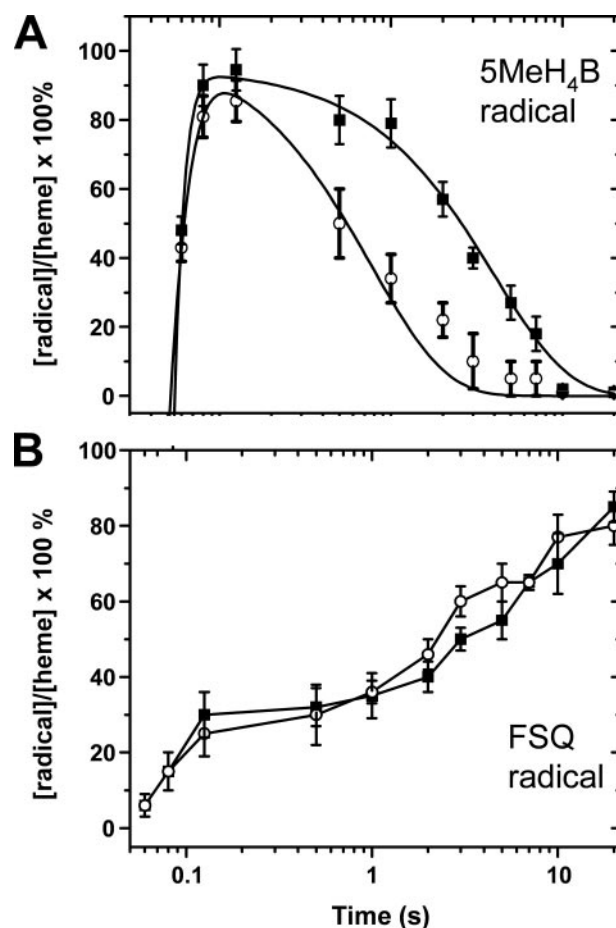


FIGURE 6. **Kinetics of 5MeH₄B and FSQ radical formation and disappearance during Arg hydroxylation reactions catalyzed by nNOS.** A solution containing 120 μM ferrous nNOS, 5MeH₄B, and Arg was mixed at 10 °C with an O₂-saturated buffer in each reaction. Data points were normalized for sample dilution. Panel A shows the calculated 5MeH₄B radical concentration per heme versus time in the Arg hydroxylation reactions catalyzed by CaM-free (solid square) and CaM-bound (open circle) nNOS. The solid lines are the best fit derived using a kinetic equation of $A \rightarrow B \rightarrow C$. Panel B shows the calculated FSQ radical concentration per heme versus time in the same nNOS reaction samples described in panel A. Data are the mean and S.D. of three individual experiments each.

Fig. 6B displays the evolution of FSQ radical content in the same nNOS reaction samples. The CaM-free and CaM-bound reactions had relatively similar FSQ radical content across the entire measurement period. A similar FSQ radical buildup was observed in replica reactions that used H₂B-saturated nNOS (data not shown).⁴ Possible reasons for this behavior are mentioned under "Discussion." In any case, the buildup of the FSQ radical was more gradual compared with the 5MeH₄B radical and occurred mostly after a majority of the 5MeH₄B radical signal had disappeared in the CaM-bound nNOS reaction.

To determine whether disappearance of the pterin radical signal in the above reactions involved the reduction or oxidation of the pterin radical, we utilized a standard HPLC fluorescence method (22) to measure the final oxidation state of H₄B in replica nNOS reaction samples that had gone to completion. In the CaM-bound nNOS reaction samples, we observed no net

⁴ H₂B-bound nNOS was used in replicated reactions to exclusively monitor FSQ radical formation (i.e. no H₄B radical can be formed).

NOS Reduces a Tetrahydrobiopterin Radical

oxidation of total H_4B ($97 \pm 3\%$ was still present as the fully reduced form), whereas in the CaM-free nNOS reaction samples, a significant portion of the total H_4B ($35 \pm 6\%$) had become oxidized. This extent of H_4B oxidation is somewhat less but similar to what was reported for single turnover Arg hydroxylation reactions catalyzed by nNOSoxy under similar conditions ($\approx 65\%$ H_4B oxidized) (13).⁵ Control reactions that either contained no enzyme or contained a CaM-free ferric (instead of ferrous) enzyme plus H_4B all had $>95\%$ of their H_4B remain in fully reduced form after reacting. Likewise, a control reaction of CaM-bound ferrous nNOS that contained H_2B (an oxidized form of H_4B) generated no H_4B during the reaction (data not shown). Together, the data indicate that the H_4B radical signal disappears through a reductive pathway in the CaM-bound nNOS reaction.

DISCUSSION

A H_4B radical forms in NOS enzymes during Arg hydroxylation, and is proposed to be reduced back to H_4B before the enzyme can convert bound NOHA to NO (Fig. 1). Here, we developed a means to investigate the pterin radical reduction step in nNOS, to validate that the process occurs, to measure the kinetics, and to determine whether pterin radical reduction is CaM-dependent.

Our results provide the first direct evidence for a NOS-catalyzed reduction of its bound pterin radical (5Me H_4B radical). Moreover, the rate we measured for the reduction (1.3 s^{-1} at 10°C) argues that it is kinetically competent, *i.e.* pterin radical reduction is fast enough to circumvent the slower and irreversible oxidation of the bound pterin radical, which occurs at 0.2 s^{-1} in nNOS at 10°C (12). The measured rates of these two opposing redox transformations now provide a kinetic rationale for H_4B redox cycling in NOS enzymes, and thus explain how one H_4B molecule tightly bound in NOS enables the enzyme to produce a greater than stoichiometric amount of NO (1, 2, 6–8, 28).

Besides rapidly binding to the nNOS heme, O_2 likely oxidized some nNOS FMN hydroquinone in our reactions after mixing.⁶ This may help explain why the time course and extent of FSQ radical buildup is similar in both enzyme reactions (*i.e.* \pm CaM) in Fig. 6. Because there was excess NADPH present in our reactions, any nNOS FSQ that formed also had a probability of becoming reduced during the reaction, and these complexities preclude our deriving clear mechanistic information from the FSQ levels that are indicated in Fig. 6.

Depending on the relative rates, a reaction between O_2 and the FMN hydroquinone could conceivably slow down the observed rate of 5Me H_4B radical reduction in our nNOS reac-

tions compared with the true maximal rate. Although this would not alter the conclusions of our present study, further work should be done to address this possibility. Also, because our analysis is based on differential relaxation rates of the pterin and FSQ radicals, it relies on these properties remaining fairly constant during the enzyme changes that occur in our reactions. The physical basis for the faster relaxation of the pterin radical is unknown, although proximity to heme is a reasonable possibility. Importantly, the relaxation properties of the nNOS heme are unlikely to change during the critical time frame of our reactions.⁷

The NOS-catalyzed regeneration of H_4B differs in fundamental ways from other NADPH-dependent reductases that regenerate H_4B (2). For example, the dihydropteridine and dihydrofolate reductases each bind an oxidized pterin substrate and release a reduced pterin product with each catalytic turnover. They also catalyze a two-electron reduction of their dihydropterin substrates. In contrast, NOS enzymes are incapable of reducing dihydrobiopterin (28) and instead catalyze a one-electron reduction of the H_4B radical, with product remaining bound in the enzyme. Thus, our data confirm the long-standing proposal that NOS enzymes may catalyze a novel reductive transformation of pterin radical in biology (8, 29).

In considering the possible mechanisms for pterin radical reduction, it is important to note that only CaM-bound nNOS was able to reduce the 5Me H_4B radical during the Arg hydroxylation reaction. Such a dependence on CaM implicates the NOS flavoprotein domain in the process. Its participation as an electron donor would be consistent with NADPH utilization measures that predicted an NADPH-derived electron would be utilized for H_4B radical reduction during the course of NO synthesis (1, 2). There also is ample precedent for CaM-dependent electron transfer in NOS, because CaM triggers ferric heme reduction by the flavoprotein domain (16, 17). CaM-dependent heme reduction in NOS enables O_2 binding and commits the enzyme toward NO synthesis (Fig. 1). Thus, our current work reveals that the NOS flavoprotein domain actually catalyzes two distinct reductions during NO synthesis, one to reduce the ferric heme and another to reduce the H_4B radical. But how similar are these processes from an enzyme structure activity viewpoint? We know that both events are CaM-dependent and involve a one-electron transfer to an acceptor molecule that is bound within the NOS oxygenase domain. We know that the hydroquinone form of FMN (FMNH₂) reduces the NOS ferric heme (19, 30), and thermodynamic considerations suggest the same probably holds for NOS pterin radical reduction (31–33). However, H_4B is bound relatively far from the protein surface near the center of the NOSoxy dimer, whereas the bound heme has an edge placed within a few Angstroms of the protein surface (34). In addition, electron transfer

⁵ Pterin radical oxidation is always less than 1 per heme in the single turnover reactions, because a significant fraction of total reduced pterin in the reaction sample is unbound and therefore not subject to NOS-catalyzed redox transformations.

⁶ We utilized buffer saturated with O_2 in our mixing experiments to insure the fastest possible heme-dioxy formation in nNOS at the start of the reaction. Thus, the initial O_2 concentration after mixing was about 0.8 mM, while the enzyme concentration (with nearly 1 FMN hydroquinone per heme) is 60 μM . Our unrelated work (R. Ilagan and D. Stuehr, unpublished results) indicates that at these relative concentrations, reaction of O_2 with the nNOS FMN hydroquinone becomes kinetically significant.

⁷ We know that pterin radical formation in nNOS occurs with coincident formation of ferric heme during Arg hydroxylation (12). In the subsequent 2 s required for pterin radical reduction (Fig. 6), the ferric heme is likely to quickly transfer an electron to the pterin radical with little or no "resident time" of the electron on the heme. Thus, all enzyme molecules that contain a pterin radical predominantly exist in ferric form until the pterin radical becomes reduced.

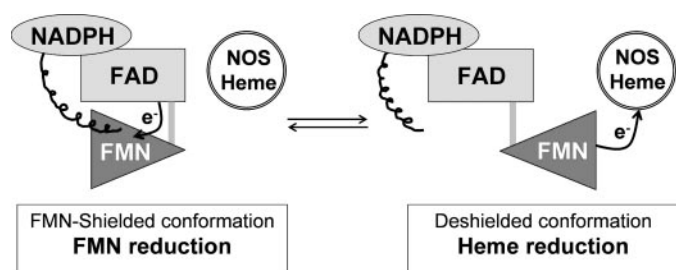


FIGURE 7. **Shuttling of the FMN module during NOS electron transfer.** The FMN module is thought to shift between an electron-accepting and an electron-donating conformation to transfer NADPH-derived electrons to the NOS oxygenase domain. The figure is adapted from Ref. 35, 44.

to the pterin and heme occur at different points in the catalytic cycle (Fig. 1), making them temporally distinct.

Regarding NOS flavin-to-heme electron transfer, a variety of data (35–40) suggest the FMN module undergoes a relatively large-scale movement to contact-shuttle between the NADPH-FAD module (to receive electrons) and the oxygenase domain (to donate electrons) during catalysis (Fig. 7). An electropositive region on surface of the NOS oxygenase domain is thought to be a docking site for the FMN module during heme reduction (34, 41) (Fig. 8), and modeling indicates that an allowable movement of the FMN module could place its FMNH₂ within 9–15 Å of the heme edge (36). In this context, at least two mechanisms are possible: the FMN module delivers electrons to the heme and to the H₄B radical by two separate pathways (possibly involving two different docking sites), or instead delivers electrons along a common pathway that involves a single docking site. We believe a two-pathway model is less likely because it would place timing and range-of-motion constraints on the FMN module that may be impossible to achieve and/or control at the protein level. For example, a modeling study of nNOS (36) indicates the FMN module cannot physically contact the oxygenase domain in areas much beyond the positive surface region indicated in Fig. 8. Although this appears to favor a common docking site model, a challenge remains regarding the electron transfer distance. The H₄B cofactor is at least 17 Å away from the implicated docking surface, and thus would be expected to get no closer than 26 to 32 Å to the FMNH₂ donor (Fig. 8). This distance is well beyond the range of edge-to-edge distances typically observed for donor and acceptor molecules in biological electron transfer systems (42), and would make timely electron transfer difficult to achieve (43).

Interestingly, the distance problem could be resolved if the NOS heme conducts the electron transfer to the H₄B radical. This would have the advantage of converting a relatively long-range electron transfer into two shorter, kinetically facile electron transfers: ~9 to 15 Å edge-to-edge from FMNH₂ to heme (36), followed by an electron transfer from heme to H₄B across a near van der Waals distance of 3 Å (Fig. 8). Indeed, such “through-heme” electron transfer is relatively common in biology (42). Under this scenario, an electron provided by the flavoprotein domain (*i.e.* FMNH₂) would always reduce the ferric heme unless the H₄B radical is present, in which case the electron would rapidly pass through the heme to reduce the H₄B radical (Fig. 8). A through-heme mechanism is consistent with NOS pterin radical reduction being CaM-dependent and its

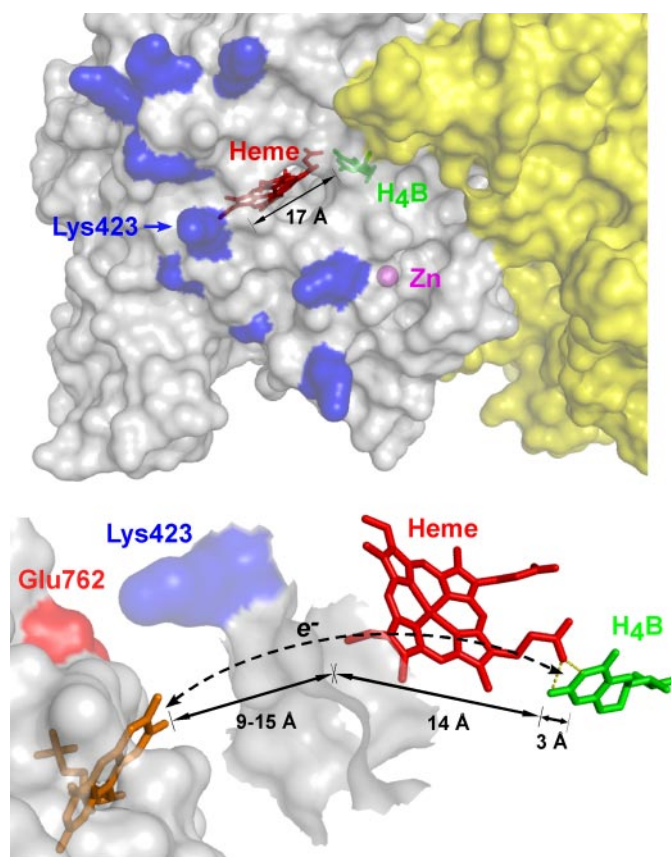


FIGURE 8. **Through-heme model for H₄B radical reduction in NOS.** Upper panel depicts the surface of a NOSoxy dimer with semi-transparent white and yellow subunits. The heme molecule (red) bound in the white subunit has an edge positioned near an electropositive surface region (blue Lys and Arg residues) that is proposed to be a docking site for the FMN module during electron transfer to the heme. Bound H₄B (green) is at least 17 Å away from this surface. Lower panel presents a closer view and shows a cartoon of the FMN module (semi-transparent white with an orange-bound FMN) interacting with the potential docking site on NOSoxy in a manner consistent with structural modeling results. A through-heme electron transfer from bound FMN to the H₄B radical (dashed line) is indicated, along with the relevant distances marked by arrows. The figure was constructed using Protein Data Bank structures 1ZVL (for rat nNOSoxy domain) and 1TLL (for rat nNOS FMN domain).

being temporally distinct from ferric heme reduction (Fig. 1). The model is also consistent with the NOS heme and (estimated) H₄B radical midpoint potentials (31–33), which indicate a strong positive driving force would exist for through-heme pterin radical reduction by the NOS flavoprotein domain.

The through-heme model also infers a number of testable predictions. For example, the rate of H₄B radical reduction may approach but should not exceed the rate of ferric heme reduction that is observed in a given NOS. This prediction holds in our nNOS experiments, where the observed rate of 5MeH₄B radical reduction at 10 °C (1.3 s⁻¹) was a bit slower but generally similar to the rate of ferric heme reduction measured at the same temperature (3 to 4 s⁻¹) (19, 44). Further investigations are underway to describe the mechanism and regulation of this novel radical reduction in the NOS enzymes.

Acknowledgments—We thank Deborah Durra for excellent technical assistance and thank members of the Tainer and Getzoff laboratories for helpful discussions.

NOS Reduces a Tetrahydrobiopterin Radical

REFERENCES

1. Gorren, A. C. F., and Mayer, B. (2007) *Biochim. Biophys. Acta* **1770**, 432–445
2. Wei, C. C., Crane, B. R., and Stuehr, D. J. (2003) *Chem. Rev.* **103**, 2365–2383
3. Denisov, I. G., Makris, T. M., Sligar, S. G., and Schlichting, I. (2005) *Chem. Rev.* **105**, 2253–2277
4. List, B. M., Klosch, B., Volker, C., Gorren, A. C. F., Sessa, W. C., Werner, E. R., Kukovetz, W. R., Schmidt, K., and Mayer, B. (1997) *Biochem. J.* **323**, 159–165
5. Gorren, A. C. F., List, B. M., Schrammel, A., Pitters, E., Hemmens, B., Werner, E. R., Schmidt, K., and Mayer, B. (1996) *Biochemistry* **35**, 16735–16745
6. Reif, A., Frohlich, L. G., Kotsonis, P., Frey, A., Bommel, H. M., Wink, D. A., Pfeleiderer, W., and Schmidt, H. H. (1999) *J. Biol. Chem.* **274**, 24921–24929
7. Giovanelli, J., Campos, K. L., and Kaufman, S. (1991) *Proc. Natl. Acad. Sci. U. S. A.* **88**, 7091–7095
8. Witteveen, C. F. B., Giovanelli, J., and Kaufman, S. (1999) *J. Biol. Chem.* **274**, 29755–29762
9. Hurshman, A. R., Krebs, C., Edmondson, D. E., and Marletta, M. A. (2003) *Biochemistry* **42**, 13287–13303
10. Berka, V., Yeh, H. C., Gao, D., Kiran, F., and Tsai, A. L. (2004) *Biochemistry* **43**, 13137–13148
11. Schmidt, P. P., Lange, R., Gorren, A. C. F., Werner, E. R., Mayer, B., and Andersson, K. K. (2001) *J. Biol. Inorg. Chem.* **6**, 151–158
12. Wei, C. C., Wang, Z. Q., Durra, D., Hemann, C., Hille, R., Garcin, E. D., Getzoff, E. D., and Stuehr, D. J. (2005) *J. Biol. Chem.* **280**, 8929–8935
13. Wei, C. C., Wang, Z. Q., Hemann, C., Hille, R., and Stuehr, D. J. (2003) *J. Biol. Chem.* **278**, 46668–46673
14. Stuehr, D. J., Kwon, N. S., Nathan, C. F., Griffith, O. W., Feldman, P. L., and Wiseman, J. (1991) *J. Biol. Chem.* **266**, 6259–6263
15. Buga, G. M., Singh, R., Pervin, S., Rogers, N. E., Schmitz, D. A., Jenkinson, C. P., Cederbaum, S. D., and Ignarro, L. J. (1996) *Am. J. Physiol.* **40**, H1988–H1998
16. Abu-Soud, H. M., and Stuehr, D. J. (1993) *Proc. Natl. Acad. Sci. U. S. A.* **90**, 10769–10772
17. Abu-Soud, H. M., Presta, A., Mayer, B., and Stuehr, D. J. (1997) *Biochemistry* **36**, 10811–10816
18. Adak, S., Ghosh, S., Abu-Soud, H. M., and Stuehr, D. J. (1999) *J. Biol. Chem.* **274**, 22313–22320
19. Panda, K., Adak, S., Aulak, K. S., Santolini, J., McDonald, J. F., and Stuehr, D. J. (2003) *J. Biol. Chem.* **278**, 37122–37131
20. Konas, D. W., Takaya, N., Sharma, M., and Stuehr, D. J. (2006) *Biochemistry* **45**, 12596–12609
21. Wei, C. C., Wang, Z. Q., Wang, Q., Meade, A. L., Hemann, C., Hille, R., and Stuehr, D. J. (2001) *J. Biol. Chem.* **276**, 315–319
22. Fukushima, T., and Nixon, J. C. (1980) *Anal. Biochem.* **102**, 176–188
23. Berka, V., Wu, G., Yeh, H. C., Palmer, G., and Tsai, A. L. (2004) *J. Biol. Chem.* **279**, 32243–32251
24. Galli, C., MacArthur, R., AbuSoud, H. M., Clark, P., Stuehr, D. J., and Brudvig, G. W. (1996) *Biochemistry* **35**, 2804–2810
25. Wei, C. C., Wang, Z. Q., Arvai, A. S., Hemann, C., Hille, R., Getzoff, E. D., and Stuehr, D. J. (2003) *Biochemistry* **42**, 1969–1977
26. Perry, J. M., Moon, N., Zhao, Y., Dunham, W. R., and Marletta, M. A. (1998) *Chem. Biol.* **5**, 355–364
27. Hurshman, A. R., Krebs, C., Edmondson, D. E., Huynh, B. H., and Marletta, M. A. (1999) *Biochemistry* **38**, 15689–15696
28. Witteveen, C. F. B., Giovanelli, J., and Kaufman, S. (1996) *J. Biol. Chem.* **271**, 4143–4147
29. Bec, N., Gorren, A. C., Voelker, C., Mayer, B., and Lange, R. (1998) *J. Biol. Chem.* **273**, 13502–13508
30. Miller, R. T., Martasek, P., Omura, T., and Masters, B. S. S. (1999) *Biochem. Biophys. Res. Commun.* **265**, 184–188
31. Gorren, A. C. F., Kungl, A. J., Schmidt, K., Werner, E. R., and Mayer, B. (2001) *Nitric Oxide* **5**, 176–186
32. Capeillere-Blandin, C., Mathieu, D., and Mansuy, D. (2005) *Biochem. J.* **392**, 583–587
33. Ost, T. W., and Daff, S. (2005) *J. Biol. Chem.* **280**, 965–973
34. Crane, B. R., Arvai, A. S., Ghosh, D. K., Wu, C., Getzoff, E. D., Stuehr, D. J., and Tainer, J. A. (1998) *Science* **279**, 2121–2126
35. Konas, D. W., Zhu, K., Sharma, M., Aulak, K. S., Brudvig, G. W., and Stuehr, D. J. (2004) *J. Biol. Chem.* **279**, 35412–35425
36. Garcin, E. D., Bruns, C. M., Lloyd, S. J., Hosfield, D. J., Tiso, M., Gachhui, R., Stuehr, D. J., Tainer, J. A., and Getzoff, E. D. (2004) *J. Biol. Chem.* **279**, 37918–37927
37. Feng, C. J., Tollin, G., Hazzard, J. T., Nahm, N. J., Guillemette, J. G., Salerno, J. C., and Ghosh, D. K. (2007) *J. Am. Chem. Soc.* **129**, 5621–5629
38. Roman, L. J., and Masters, B. S. (2006) *J. Biol. Chem.* **281**, 23111–23118
39. Daff, S. (2003) *Biochem. Soc. Trans.* **31**, 502–505
40. Dunford, A. J., Rigby, S. E. J., Hay, S., Munro, A. W., and Scrutton, N. S. (2007) *Biochemistry* **46**, 5018–5029
41. Shimanuki, T., Sato, H., Daff, S., Sagami, I., and Shimizu, T. (1999) *J. Biol. Chem.* **274**, 26956–26961
42. Page, C. C., Moser, C. C., and Dutton, P. L. (2003) *Curr. Opin. Chem. Biol.* **7**, 551–556
43. Moser, C. C., Page, C. C., and Dutton, P. L. (2006) *Philos. Trans. R. Soc. Lond., B, Biol. Sci.* **361**, 1295–1305
44. Tiso, M., Konas, D. W., Panda, K., Garcin, E. D., Sharma, M., Getzoff, E. D., and Stuehr, D. J. (2005) *J. Biol. Chem.* **280**, 39208–39219